



Nanoscale

**Towards the Identification of the Gold Binding Region
within Trypsin Stabilized Nanoclusters using Microwave
Synthesis Routes**

Journal:	<i>Nanoscale</i>
Manuscript ID	NR-ART-10-2020-007068.R1
Article Type:	Paper
Date Submitted by the Author:	06-Dec-2020
Complete List of Authors:	Griep, Mark; US Army Research Laboratory, WMRD Sellers, Michael ; US Army Research Laboratory Weapons and Materials Research Directorate Subhash, Bijil; University of New South Wales, School of Chemical Engineering Fakner, Alexis ; US Army Research Laboratory Weapons and Materials Research Directorate West, Abby ; US Army Research Laboratory Weapons and Materials Research Directorate Bedford, Nicholas; University of New South Wales Faculty of Engineering,

SCHOLARONE™
Manuscripts

Towards the Identification of the Gold Binding Region within Trypsin Stabilized Nanoclusters using Microwave Synthesis Routes

Mark H. Griep[†], Michael S. Sellers[†], Bijil Subhash[‡], Alexis M. Fakner[†], Abby L. West[†],

Nicholas M. Bedford^{‡*}

[†] Weapons and Materials Research Directorate, CCDC Army Research Laboratory,

Aberdeen Proving Ground, MD 21005, USA

[‡]School of Chemical Engineering, University of New South Wales, Sydney, NSW 2052,

Australia

*Corresponding author: n.bedford@unsw.edu

Abstract

Elucidating the location of stabilized nanocluster within their protein hosts is an existing challenge towards the optimized development of functional protein-nanoclusters. While nanoclusters of various metal compositions can be readily synthesized within a wide array

of protein hosts and exhibit tailorable properties, the inability to identify the cluster stabilization region prevents controllable property manipulation of both metallic and protein components. Additionally, the ability to synthesize protein-nanoclusters in a consistent and high-throughput fashion is also highly desirable. In this effort, trypsin stabilized gold nanoclusters are synthesized through standard and microwave-enabled methodologies to determine the impact of processing parameters on the materials physical and functional properties. Density functional theory simulations are employed to localize high probability regions within the trypsin enzyme for Au₂₅ cluster stabilization, which reveal that cluster location is likely within close proximity of the trypsin active region. Trypsin activity measurements support our findings from DFT, as trypsin enzymatic activity is eliminated following cluster growth and stabilization. Moreover, studies on the reactivity of Au NCs and synchrotron characterization measurements further reveal that clusters made by microwave-based techniques exhibit slight structural differences to those made via standard methodologies, indicating that microwave-based syntheses largely maintain the native structural attributes despite the faster synthetic conditions. Overall, this work illustrates the importance of understanding the connections between

synthetic conditions, atomic-scale structure, and materials properties that can be potentially used to further tune the properties of metal cluster-protein materials for future applications.

Introduction

Composed of metal atoms ranging from fewer than ten to several hundred atoms, metal nanoclusters (NC)s exhibit quantized energy fluorescence similar to quantum dots (QD)s due to their small diameter as opposed to the plasmons associated with the continuous density of states in noble metal nanoparticles.¹⁻³ The discrete energy levels allow for tuneable photonic emission in the visible and IR regions, highly efficient two-photon absorption, and quantum yields exceeding 6%.⁴ Recent advances in metallic nanoclusters have demonstrated their applicability in diverse applications, such as biolabelling and bioimaging, where nanoclusters can interact with metal ions,⁵ proteins,^{4, 6-11} nucleic acids,^{5, 9, 10, 12} and small biomolecules.¹¹ More recently, expanded functionality and materials design strategies have been achievable through protein-stabilized NC (PNC) growth/encapsulation methodologies.¹³ These include the ability to engineer 2D/3D NC structures¹⁴⁻¹⁶ and perform *in vivo* physiological targeting/monitoring.¹⁷ In the majority of these studies the stabilizing protein host largely serves as a scaffold for the nanocluster, without any enhancement/monitoring of the native activity of the protein.

With proper engineering of the hybrid system, opportunities exist to harness the capabilities/functionality of both the nano and bio components in both independent and cooperative systems. In the case of enzyme-nanocluster systems, it has been shown that the growth

of nanoclusters within DNASE-I does not inhibit the enzymes native protease activity and, in fact, can directly monitor the enzymatic activity through modulation of the nanocluster emission.¹⁸ While the enzyme-nanocluster system proved functional in this specific case, the ability to determine or selectively control the nanocluster stabilization region within a host protein so as to not interfere with the native enzymatic/biological activity has yet to be achieved. In this work, we employ a series of experimental and computational methods to understand structure/function relationships in PNCs using the enzyme trypsin as a model protein host for both traditional and microwave-assisted synthesis methods. While a multitude of enzymes or ion-pumping proteins would be of interest to study potential interactions of associated nanoclusters on their innate biological activity, a trypsin-AuNC model was chosen due its' representation of the large family of proteases, a clear understanding of the trypsin enzymatic mechanism,¹⁹ and the previous demonstration of the trypsin-AuNC hybrid synthesis for reference.^{20,21} With a well-defined active region and understanding of the key functional amino acids associated with the catalytic triad, the impact of nanocluster growth on trypsins' enzymatic active could help infer cluster binding location.

We discover that microwave-assisted synthesis methods result in Au PNCs that are similar in structure using a combination of X-ray absorption spectroscopy (XAS) and high-energy X-ray diffraction (HE-XRD) coupled to atomic pair distribution function analysis (PDF). Moreover, the similarity in structures results in similar optical properties between the two trypsin-based PNCs and also exhibits similar reactivity toward the 4-nitrophenol reduction reaction. Computational modeling efforts indicate Au cluster binding predominately located near the cysteine at the enzymatic binding site, which was further substantiated by a complete loss of enzymatic reactivity. Overall these results showcase the ability to make Au PNCs using microwave-assisted synthetic

strategies that do not drastically perturb cluster structure or properties, potentially enabling larger scale production on these emerging materials, while also elucidating the most likely binding site of Au₂₅ within a trypsin host.

Results and Discussion

Trypsin-stabilized Au PNCs were synthesized by traditional synthetic routes (12 h) and microwave-assisted synthesis methods (~5 s), as illustrated in Figure 1.²⁰ As described in more detail in the Experimental section, the only difference between the two syntheses chosen here is the mode of heating and associated shorter time scale through the use of microwave heating. As such, microwave synthesis can potentially provide functional materials under much faster synthesis times. The impact of these two synthesis methodologies on Au PNC formation within the trypsin protein was probed using a series of experimental methods. While established protocols have shown the ability to achieve high quality NC growth in a wide-array of protein hosts; new avenues for increasing future production rates are still needed for eventual translation into real-world applications. Microwave chemistry has been demonstrated to be an effective methodology to drive and control PNC formation,²²⁻²⁵ however this is the first report of trypsin-AuNC material synthesis through this approach. While microwave-based PNC synthesis approaches have yielded high-quality fluorescent products similar to that of traditional wet-chemistry synthetic methods; tailoring highly functional hybrids is still elusive due to the lack of fundamental knowledge on the precise cluster stabilization region and cluster-ligand interaction within the host protein. Exploring both synthesis routes in this work allows for evaluation of potential differences in the nanocluster formation process and stabilization region with the host protein and provides further clarification if these differing methods provide homologous materials.

Initial inspection of the fluorescence emission of the prepared nanoclusters reveals similar spectral outputs, as shown in Figure 2(a). The fluorescence emission peak around $\lambda_{650\text{nm}}$ remains consistent with both synthesis methodologies, likely indicating similar nanocluster formation and stabilization mechanisms are similar. Previous reports of trypsin-AuNC synthesis have verified that the emission peak around $\lambda_{650\text{nm}}$ corresponds to an Au₂₅ cluster with a diameter of $\sim 2\text{nm}$ ^{20, 21}. Furthermore, circular dichroism (CD) spectroscopy measurements reveal that trypsin loses all secondary protein structure upon NC synthesis in both methodologies, instead showcasing a random coil morphology (Figure 2(b)). This finding indicates that the presence of Au NCs influence protein structure, but not the employed synthetic conditions. The loss of trypsin secondary structure in coordination with the presence of metal ions has been previously shown²⁶, thus Au ion binding and subsequent nanocluster formation is expected to have a direct impact on α -helix and β -sheet composition. Notably, the synthesis method was found to have no significant impact on other Au PNC hybrids tested as well, including BSA, lysozyme, and pepsin protein hosts (Figure S1 and Figure S2).

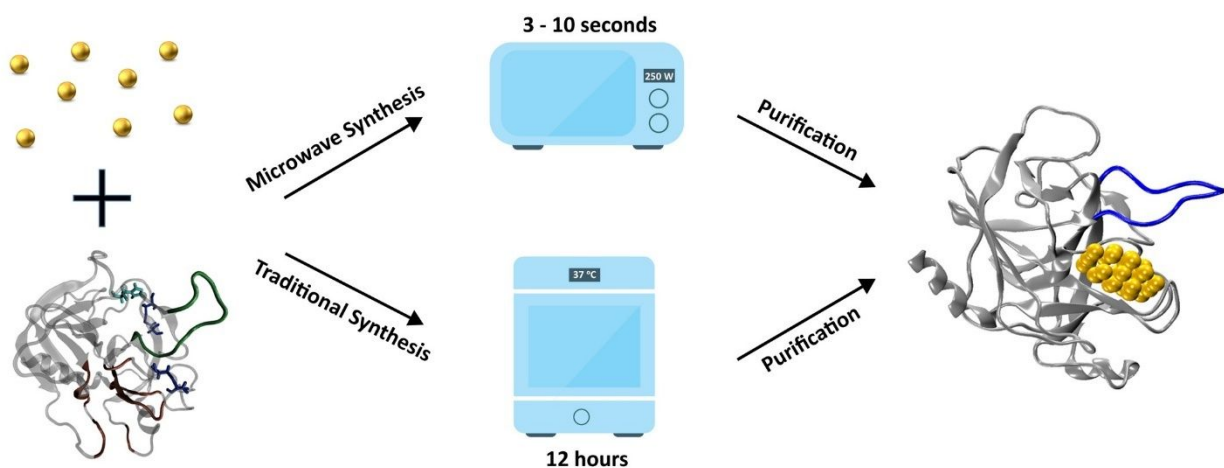


Figure 1. Schematic of the two synthetic routes chosen to generate trypsin-based Au-PNCs.

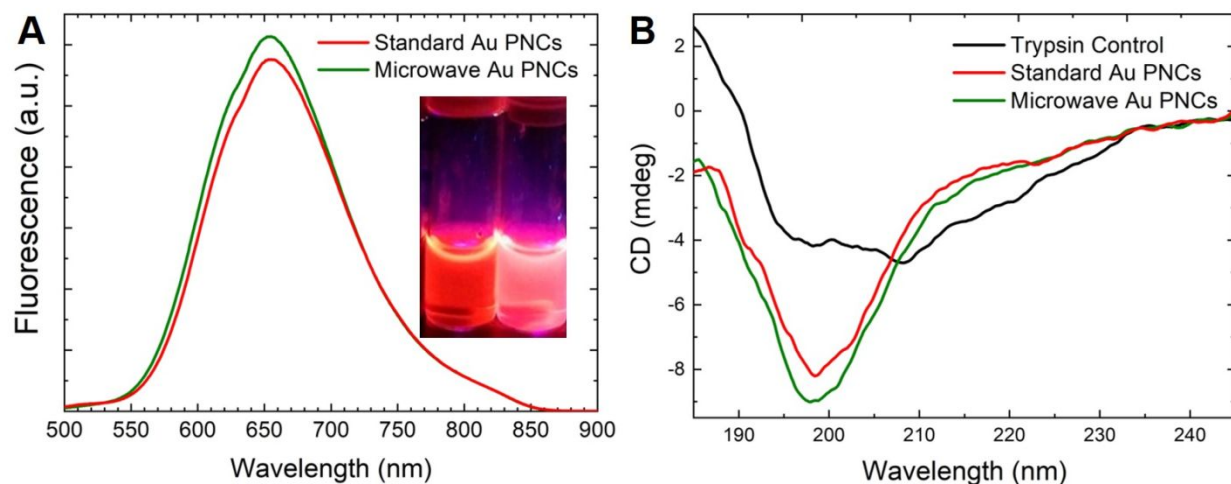


Figure 2. Comparison of trypsin Au PNCs synthesized with standard and microwave methods, evaluating (a) fluorescence emission and (b) CD spectra

To better understand the local atomic environment around the Au PNCs, XAS measurements were performed at the Au L₃-edge (Figure 3). The X-ray absorption near-edge structure (XANES) demonstrate that both trypsin PNCs from standard and microwave-assisted syntheses exhibit a drastic departure from that of bulk Au (Figure 3a). Features in the XANES for both PNCs are broad due to the lack of longer-range order and are consistent with clusters previously reported in the literature.²⁷⁻³⁰ Slight increases in white line intensity and E₀ (~ + 0.5 eV) indicate a small population of oxidized Au atoms with clusters, which is expected given the large surface area of the cluster and their associated interactions with the host protein. Figure 3b shows the extended X-ray absorption fine-structure (EXAFS) data for the trypsin PNCs along with a reference Au foil, which provide a more immediate and intuitive understanding of the local Au structure. EXAFS were obtained following conversion of the XAS data to *k*-space (*k*²-weighted, Figure S3), and Fourier transformed from 2.0 to 12.0 Å⁻¹. For the Au foil, the split peak arising from Townsend-Ramsauer resonance represent the first coordination sphere of Au-Au atoms in bulk Au. Notably, the first major peak for both trypsin PNCs is located at 1.89 Å (not corrected

for phase shift). This distance has been previously identified to be arising from Au cluster-protein interactions, most likely with S-atoms in cysteine residues.²⁷⁻²⁹ Longer radial distances of 2.42 and 2.75 Å correspond to the Au-Au distances within the clusters, which is significantly truncated when compared to bulk or nanoparticle counterparts.

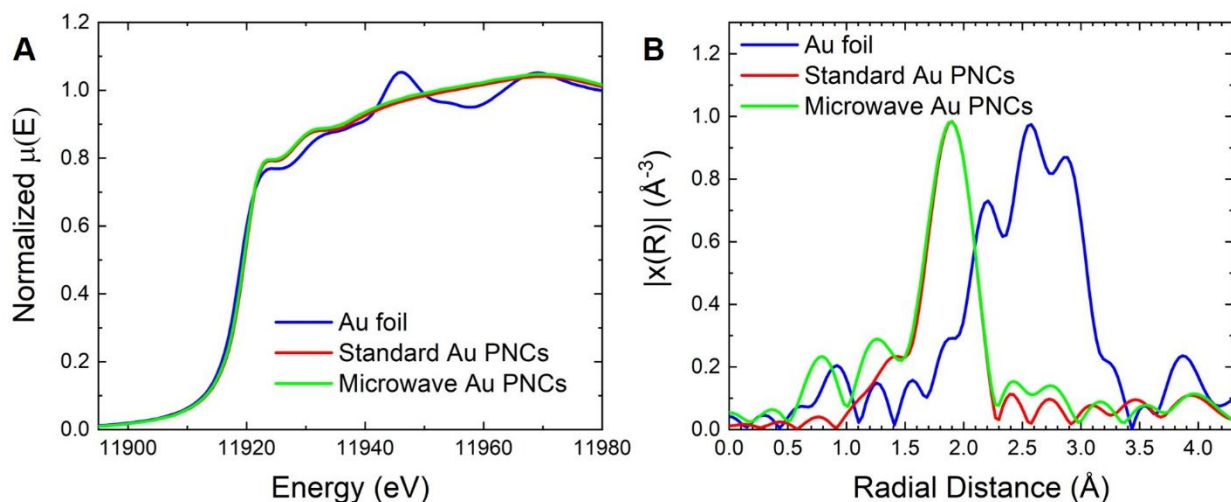


Figure 3. Au L_3 -edge a) XANES and b) EXAFS for trypsin Au PNCs synthesized using standard method (red line) and microwave-assisted method (green line) along with a reference Au foil

EXAFS modeling was performed to obtain local average Au coordination numbers (CNs) and nearest neighbor distances as described in the experimental section. EXAFS fittings results are shown in Figure S4 in the supporting information and summarized in Table 1. The Au-protein CN, representative of all possible protein interactions due to the differences in atomic mass of Au, is approximately ~ 2 for both Au trypsin PNCs synthesized via standard and microwave-assisted techniques (2.04 ± 0.28 and 1.92 ± 0.14 respectively). The Au-Au CN is slightly smaller in the PNCs made via standard synthesis techniques (1.15 ± 0.42) than the microwave assisted PNCs (1.46 ± 0.36), suggesting that cluster size is slightly larger in the latter materials, likely due to the rapid heating and nucleation mechanisms that occur in the microwave assisted techniques.^{31, 32} It is important to note that the local coordination in both materials is different to those previously

reported on thiolated Au clusters and similar materials, wherein a CN of ~ 1.0 is reported for Au-ligand interactions and a Au-Au CN higher than 2.0 is reported for various different cluster syntheses.³³⁻³⁵ These results indicate that Au-trypsin interactions occur from multiple residues in the first coordination sphere of the surface Au atoms in the PNCs vs the use of thiol-containing organic linkers. The significantly reduced CNs in the PNCs compared to previously reported thiolated clusters strongly indicates a lack of ordering in the cluster, which is somewhat expected given the larger number of possible binding functionalities within trypsin vs designer thiolated clusters. The average Au-Protein NNDs is ~ 2.3 Å for both trypsin PNCs while Au-Au NNDs are also similar for both materials. For comparison purposes, EXAFS modeling efforts from previous Au NCs is summarized in Table S1.^{27-29, 34-36} Overall, the XAS data demonstrates that minor structural changes occur when microwave assisted syntheses techniques are used over standard synthetic methods, indicating minimal influence of microwave-based processes in the creation of Au PNCs.

Table 1. Summary of EXAFS fitting results.

Au NC	Au-Protein CN	Au-Au CN	Au-Protein NND (Å)	Au-Au NND (Å)	Au-Protein σ^2	Au-Au σ^2	R-factor
Traditional Synthesis	2.04 \pm	1.15 \pm	2.317 \pm	2.79 \pm	0.003 \pm	0.008 \pm	0.00081
Microwave Synthesis	1.92 \pm	1.46 \pm	2.309 \pm	2.78 \pm	0.002 \pm	0.002 \pm	0.0026
	0.14	0.36	0.003	0.03	0.001	0.001	

To further explore the longer-range structure of the trypsin-based Au-PNCs, atomic PDF analysis was performed on Au-PNCs and trypsin powder (Figure 4). Atomic PDFs provide longer range atomic-scale structural information independent of periodicity, which is ideal for studying

nanoscale materials.^{37, 38} The PDFs revealed that both the standard and microwave synthesis methods yield PNCs of similar atomic structure at longer length scales, as shown in Figure 4 and Figure S5. The longer-range order extends past the size of the Au PNCs (Figure S5), suggesting the protein-protein and Au-protein atomic pairs are prevalent in their respective PDFs. Indeed, the first major peak in the Au PNCs at 1.38 Å is an aggregation of common bond lengths in proteins and is also found in the PDF for trypsin powder. For reference, the atomic PDFs for peptide-capped Au NPs using the AuBP1 peptide is also shown in Figure 4 and Figure S5.³⁹ It is clear that the Au PNCs do not resemble fcc-type Au as compared to AuBP1-capped Au nanoparticles, and more importantly, do not exhibit major peak shifts across the available radial distribution space that would signify significant structural changes. Differences in peak intensities and peak full width half max values can provide some insights into the relative degree of ordering between these materials, wherein the microwave-assistance Au PNCs exhibit slight increases in relative peak intensity. This suggest there is likely some increase in local structural order in this material, consistent with EXAFS results.

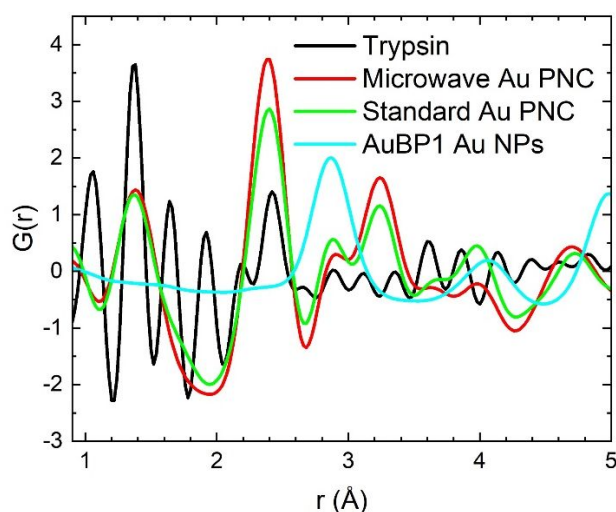


Figure 4. PDF analysis comparing control trypsin, a peptide-capped Au nanoparticle (AuBP1), standard trypsin-Au PNCs, and microwave trypsin Au PNCs.

With confirmation that the structural and photophysical properties of the trypsin Au PNCs remain largely unchanged between the microwave-assistance synthesis and traditional PNC synthetic methods, computational energetic and protein displacement data were generated to determine probable gold nanocluster growth locations within the trypsin protein. Results for the top sites identified by greatest free energy difference are listed in Table 2 with corresponding locations highlighted in the protein model in Figure 5. The simulated cluster in the top ranked stabilization location is shown in Figure 5b. The models predict, as schematically shown in Figure 6(a), that the highest probability cluster location is in close proximity to the active site of the trypsin enzyme. As a serine protease, the enzymatic function of trypsin is the result of a coordinated catalytic triad involving the histidine-57, aspartate-102, and serine-195 amino acid residues. As the serine-195 residue is known to be the most directly involved in the catalytic activity,⁴⁰ coordinating the serine-195 residue with the nanocluster stabilization would reduce its effectiveness at forming the required oxyanion hole, resulting in an increased energy barrier for reaction kinetics. It is thus hypothesized that Au PNCs synthesized by trypsin in a location close to the enzyme's active site could alter the protein's native function. As shown in Figure 6(b), a significant disruption of enzymatic activity upon cluster formation is verified. In fact, here it is shown that a complete loss of trypsin enzymatic activity is lost upon NC growth/stabilization within the trypsin molecule. The loss of enzymatic activity supports simulation predictions that the cluster stabilization region is in direct proximity to the enzymatic active region. As the loss of activity is measured in both standard and microwave-synthesized trypsin Au PNC systems, the cluster stabilization region and subsequent cluster-ligand interactions are likely similar.

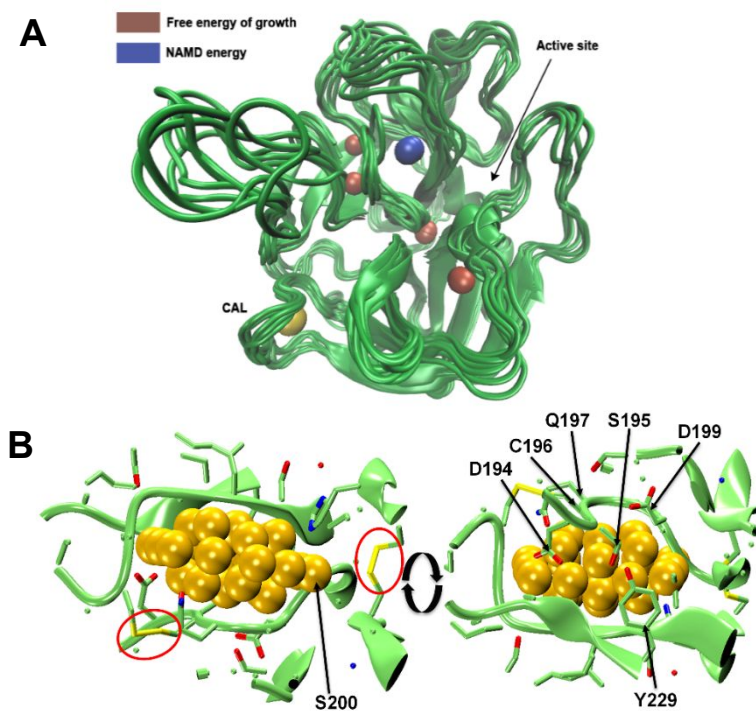


Figure 5. (a) Growth regions highlighted in protein model. (b) Probable AuNC binding pocket in trypsin with associated ligands highlighted.

Table 2: Energetic and protein displacement data at high probability cluster growth regions.

Growth Site #	Free Energy (kcal mol ⁻¹)	NAMD Energy (kcal mol ⁻¹)	Total Displacement of Protein (Å)
68	-34.32	-104.20	1.95
116	-32.30	-64.25	2.16
58	-31.98	-66.50	1.81
126	-31.93	-97.40	2.14
50	-31.72	-70.79	1.96

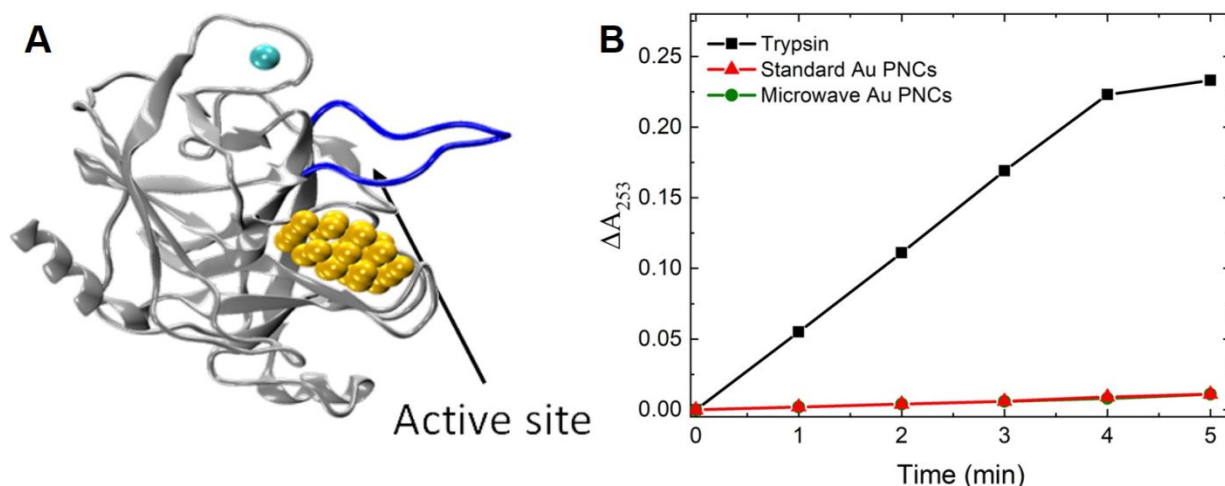


Figure 6. (a) Schematic of AuNC binding location in trypsin with respect to active site and (b) comparison of trypsin enzymatic activity in control and hybrid conformations.

To further probe the structural similarity between the two trypsin Au PNCs, catalytic activity was tested using 4-nitrophenol (4-NP) reduction reaction, a thermodynamically feasible but kinetically restricted reaction in the absence of a catalyst. In the presence of catalyst, the reduction of 4-NP can be understood using a Langmuir-Henshelwood model, where reactants, 4-NP and surface-hydrogen species (derived from NaBH_4) are adsorbed on the surface of the catalyst to facilitate the formation of 4-aminophenol.⁴¹ The kinetics of 4-NP reduction was probed using time-resolved UV-Vis spectroscopy, which demonstrated a gradual decay of the characteristic 4-NP peak (400 nm) with a concomitant increase in 4-AP peak (300 nm), as shown in Figure 7a for the microwave synthesized Au PNCs. The presence of isosbestic points in the UV-Vis spectra indicates that the reaction proceeds without the formation of any unwanted by-products.⁴² Owing to the fast reaction and the high concentration of BH_4^- ions, the absorbance data were fit using a pseudo-first order model (Figure 7b), where the slope of the fit is the apparent rate constant of the reaction. As per the previously reported studies of similar reaction systems,⁴³ the reaction rate constants exhibited a linear dependency on the temperature (Figure 7c). The temperature

dependency of rate constant for standard Au PNCs is shown in Figure S6. Arrhenius plots of Au PNCs are shown in Figure 7d and allow for the calculation of the catalytically-driven activation energies (E_a , Table 3). The microwave synthesized Au PNCs exhibits a lower E_a (54.68 ± 5.71 kJ/mol) than the standard synthesized Au PNCs (63.85 ± 1.55 kJ/mol), indicating that reactivity is slightly improved through the use of microwave-based synthetic techniques. Given the predicted Au NC location within trypsin (Figure 6a) and the similarities in optical properties (Figure 2), protein-based influences on reactivity (impeded substrate diffusion, protein assessed reactions, etc.) can likely be ruled out. The slight increase overall Au structure using microwave assisted synthesis methods, as observed by EXAFS analysis (Figure 4 and Table 1) and PDF observations (Figure 5), is a more likely cause given the closer resemblance to fcc Au, which have exceeding lower E_a for 4-NP reduction reactions.^{39, 44}

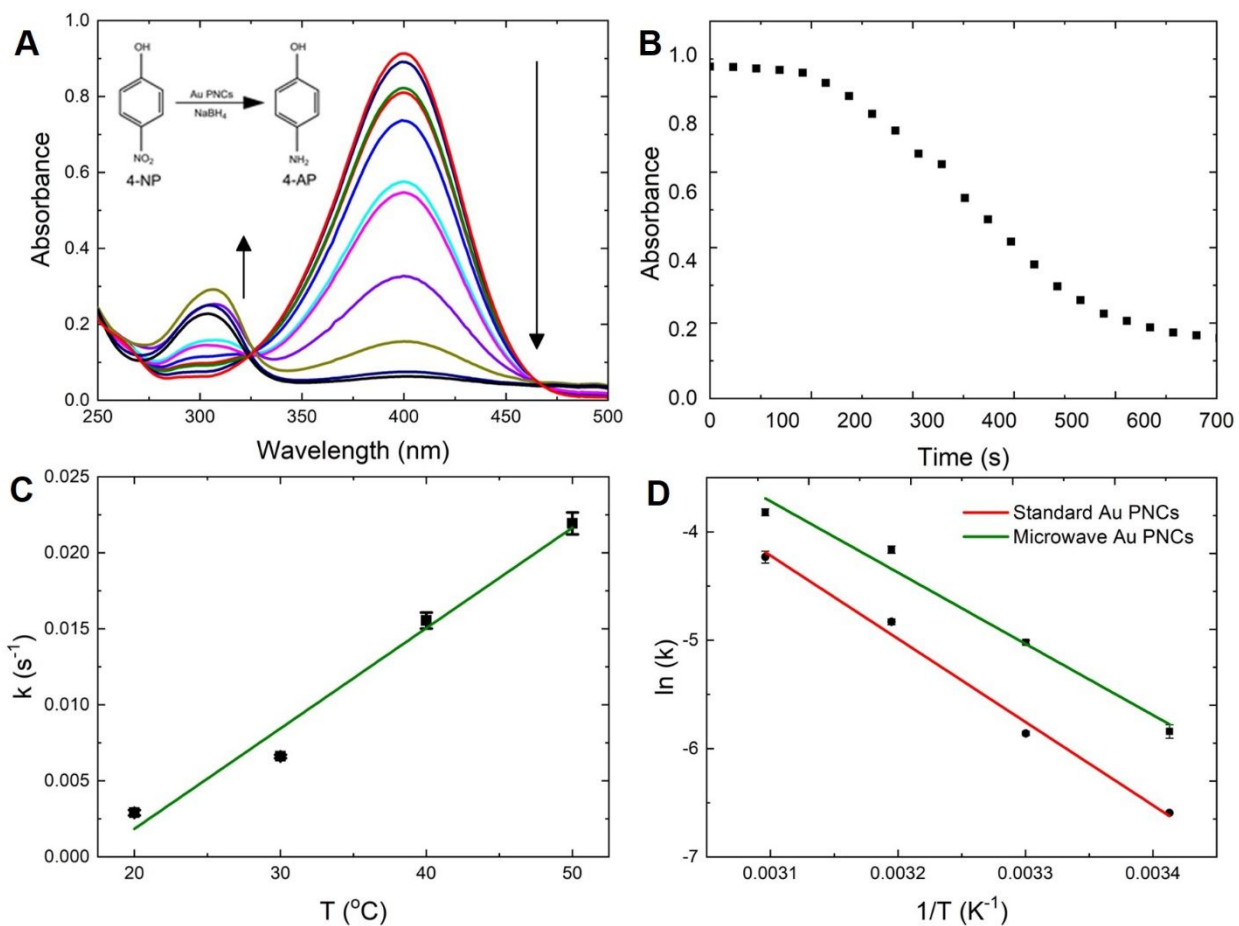


Figure 7. (a) UV-Vis Spectra of 4-NP reduction (b) Absorbance at 400 nm as a function of time (c) Apparent rate constant plotted against reaction temperature, and (d) Arrhenius plots of 4-NP reduction using Au PNC samples.

Table 3. Arrhenius Parameters of 4-NP reduction on Au PNCs.

Sample	Activation Energy (kJ mol ⁻¹)	Frequency Factor (s ⁻¹)
Standard Au PNCs	63.85 ± 1.55	1.74 × 10 ⁷
Microwave Au PNCs	54.68 ± 5.71	3.21 × 10 ⁸

Conclusion

In this work, a direct comparison of trypsin Au PNC synthesis methodologies, including traditional wet chemistry and microwave approaches, are compared and demonstrated to yield near identical products as evidenced by fluorescence, CD, and synchrotron X-ray characterization. To identify potential cluster locations with the trypsin Au PNC complex, a DFT approach is utilized, isolating the highest probability cluster stabilization region to be in direct proximity to the trypsin's active region responsible for catalytic activity. Experimental support of this cluster location is evidenced through the complete elimination of trypsin enzymatic activity within the Au PNC, suggesting the close proximity of the cluster to the active region inhibits enzymatic function. As the benefits of dual-functional PNC hybrids could serve as an enabling tool in emerging technologies, this work presents a foundation to determine cluster location within the host protein which will enable protein engineering pathways to selectively place clusters at specified regions within the protein.

Experimental

Traditional Synthesis Au PNCs

The control protein:AuNCs were synthesized with slight modifications according to previously reported methods.²⁰ In brief, hybrids were prepared by mixing aqueous protein solution (5mL, 20mM) with an aqueous solution of HAuCl₄ (5mL, 10mM) under stirring. Once mixed, the solution was adjusted to pH 12 through addition of NaOH (0.5mL, 1M). The solution is incubated at 37 °C for 12 hours under vigorous stirring. The final solution is purified of excess gold salt with a 5-kDa molecular weight cut-off (MWCO) spin filter.

Microwave Synthesis of Au PNCs

The methodology to synthesize protein:AuNCs via a microwave reactor utilizes the same starting materials as with the traditional methods. Initial solutions were prepared by mixing aqueous protein solution (5mL, 20mM) with an aqueous solution of HAuCl₄ (5mL, 10mM) under stirring. Once mixed, the solution was adjusted to pH 12 through addition of NaOH (0.5mL, 1M). A 5mL volume of the prepared solution was transferred to a microwave reaction tube and placed into a CEM Discover microwave synthesizer. The samples were reacted for 3-10 seconds at 250W. The final solution is purified of excess gold salt with a 5-kDa MWCO spin filter.

Characterization

Fluorescent emission of the protein-nanocluster hybrids was measured on a Perkin Elmer UV/Vis/NIR fluorospectrometer operating over a range of 500 to 900 nm, with a path length of 1 cm. Circular dichroism (CD) was performed according to previously published methodologies.⁴⁵ All samples were run at 25°C in a 25 mM NaH₂PO₄, 100 mM NaCl buffer at pH 7.5. Secondary structure content was evaluated on CD Pro software. X-ray absorption spectroscopy (XAS) experiments were performed at 10-BM beamline at the Advanced Photon Source (APS), Argonne National Laboratory (ANL). Aqueous PNC samples were loaded into 1 mm OD Kapton capillaries and measured in a fluorescence geometry from 200 eV below the Au L₃-edge (11.918 keV) to 1000 eV above the edge. Raw data manipulation, data reduction, and subsequent modeling were performed with the Demeter software package.⁴⁶ EXAFS model was performed using Au-S and Au-Au backscattering paths were generated using the reported structure of a thiolate protected Au₂₅ cluster, and a S₀² value of 0.844 obtained from modeling the EXAFS of a Au reference foil.³³ High energy x-ray diffraction (HE-XRD) experiments were performed at 11-ID-C beamline at the APS. Lyophilized powders of trypsin PNCs made by standard and microwave-assisted synthetic techniques were loaded into 1 mm OD Kapton capillaries along with trypsin powder for HE-XRD experiments at 105.7 keV. HE-XRD patterns were background subtracted, converted into reduced structure functions ($F(Q)$), and Fourier transformed into atomic pair distribution functions using the program RAD.⁴⁷

Catalytic Reactions

The catalytic activity of both standard and microwave stabilized Au PNC samples were studied using the model 4-nitrophenol reduction, with slight modifications to previously reported

procedure.⁴³ Briefly, 1 mL of as-synthesized Au PNC sample was mixed with 1 mL of 150 μ M 4-nitrophenol solution in a 3.5 mL quartz cuvette with 1 cm path length and left undisturbed for 5 minutes. To this solution, 1 mL of freshly prepared aqueous NaBH_4 (60 mM) was added to initiate the reaction. The extinction of 4-nitrophenol was monitored at 400 nm using Agilent Cary 8454 UV-Vis Spectrometer at 6 seconds interval for 30 minutes. Reactions were performed in triplicate at temperatures of 20, 30, 40 and 50 $^\circ\text{C}$ in order to obtain activation energies (E_a) for each catalyst.

Molecular Dynamics Simulations

A raw Au_{25} cluster was optimized using first principle ab initio quantum-chemistry package, the General Atomic and Molecular Electronic Structure System, using Density Functional Theory (DFT) with a basis set of LanL2DZ3. The coordinates of the optimized Au_{25} nanocluster were introduced within the lowest energy sites obtained using Au_{10} clusters. Molecular dynamics simulations at each of the grid points were run in parallel. Energies and the atomistic trajectories from these simulations were analyzed using the XPairIt simulator to determine: 1) the free energy required to “grow-in” a sphere representing a nanocluster; 2) the interaction energy between the sphere and the surrounding protein amino acids; 3) the total displacement of atoms from their original positions upon “growing” the sphere. The data at each site was subsequently ranked based on free energy and total displacement to determine the most probable locations for nanocluster growth.

Conflicts of Interest

There are no conflicts to declare.

Acknowledgements

This work was supported in part by an internal Directors Research Initiative at the Army Research Laboratory. B. S. would like to acknowledge scholarship support from the Research Training

Program administered by the Department of Education of the Australian Government. HE-XRD and XAS experiments were carried out at the 11-ID-C and 10-BM beamlines of the Advanced Photon Source, a U.S. Department of Energy (DOE) Office of Science User Facility operated for the DOE Office of Science by Argonne National Laboratory under Contract No. DE-AC02-06CH11357. The 10-BM beamline was further supported by the Materials Research Collaborative Access Team and its member institutions. The authors would like to thank Drs. Yang Ren and John Katsoudas for assistance at 12-ID-C and 10-BM, respectively. The authors would also like to thank Govind Mallick (ARL) for his input and efforts on protein nanocluster simulations

References

1. L. Shang, S. J. Dong and G. U. Nienhaus, *Nano Today*, 2011, **6**, 401-418.
2. J. Zheng, P. R. Nicovich and R. M. Dickson, *Annu Rev Phys Chem*, 2007, **58**, 409-431.
3. J. Zheng, C. Zhang and R. M. Dickson, *Phys Rev Lett*, 2004, **93**, 077402.
4. H. Kawasaki, K. Hamaguchi, I. Osaka and R. Arakawa, *Advanced Functional Materials*, 2011, **21**, 3508-3515.
5. W. Y. Chen, G. Y. Lan and H. T. Chang, *Anal Chem*, 2011, **83**, 9450-9455.
6. H. Wei, Z. Wang, L. Yang, S. Tian, C. Hou and Y. Lu, *Analyst*, 2010, **135**, 1406-1410.
7. X. Le Guevel, N. Daum and M. Schneider, *Nanotechnology*, 2011, **22**, 275103.
8. J. Xie, Y. Zheng and J. Y. Ying, *J Am Chem Soc*, 2009, **131**, 888-889.
9. G. Liu, Y. Shao, K. Ma, Q. Cui, F. Wu and S. Xu, *Gold Bull*, 2012, **45**, 69-74.
10. G. Liu, Y. Shao, F. Wu, S. Xu, J. Peng and L. Liu, *Nanotechnology*, 2013, **24**, 015503.
11. C. T. Chen, W. J. Chen, C. Z. Liu, L. Y. Chang and Y. C. Chen, *Chem Commun (Camb)*, 2009, DOI: 10.1039/b916919a, 7515-7517.
12. J. T. Petty, J. Zheng, N. V. Hud and R. M. Dickson, *Journal of the American Chemical Society*, 2004, **126**, 5207-5212.
13. M. H. Griep, A. L. West, M. S. P. Sellers, M. Karna, E. Zhan and N. Hoque, in *Handbook of Nanoparticles*, ed. M. Aliofkhazraei, Springer International Publishing, Cham, 2015, DOI: 10.1007/978-3-319-13188-7_33-1, pp. 1-24.
14. H. Ding, H. Li, X. Wang, Y. Zhou, Z. Li, J. K. Hiltunen, J. Shen and Z. Chen, *Chemistry of Materials*, 2017, **29**, 8440-8448.
15. M. H. Griep, J. D. Demaree, D. P. Cole, T. C. Henry and S. P. Karna, *Plasmonics*, 2020, DOI: 10.1007/s11468-019-01082-w.
16. M. H. Griep and N. M. Bedford, *Journal of Physics: Materials*, 2020, **3**, 045002.

17. A. L. West, N. M. Schaeublin, M. H. Griep, E. I. Maurer-Gardner, D. P. Cole, A. M. Fakner, S. M. Hussain and S. P. Karna, *ACS applied materials & interfaces*, 2016, **8**, 21221-21227.
18. A. L. West, M. H. Griep, D. P. Cole and S. P. Karna, *Analytical Chemistry*, 2014, **86**, 7377-7382.
19. L. Polgár, *Cellular and Molecular Life Sciences CMLS*, 2005, **62**, 2161-2172.
20. H. Kawasaki, K. Yoshimura, K. Hamaguchi and R. Arakawa, *Analytical Sciences*, 2011, **27**, 591-591.
21. Y. Xu, J. Sherwood, Y. Qin, D. Crowley, M. Bonizzoni and Y. Bao, *Nanoscale*, 2014, **6**, 1515-1524.
22. Y. Yue, T.-Y. Liu, H.-W. Li, Z. Liu and Y. Wu, *Nanoscale*, 2012, **4**, 2251-2254.
23. L. Yan, Y. Cai, B. Zheng, H. Yuan, Y. Guo, D. Xiao and M. M. F. Choi, *Journal of Materials Chemistry*, 2012, **22**, 1000-1005.
24. Y. Liu, G.-F. Tian, X.-W. He, W.-Y. Li and Y.-K. Zhang, *Journal of Materials Chemistry B*, 2016, **4**, 1276-1283.
25. K.-T. Chuang and Y.-W. Lin, *The Journal of Physical Chemistry C*, 2017, **121**, 26997-27003.
26. L. Yang, Z. Gao, Y. Cao, R. Xing and X. Zhang, *ChemBioChem*, 2005, **6**, 1191-1195.
27. M. A. MacDonald, D. M. Chevrier, P. Zhang, H. Qian and R. Jin, *The Journal of Physical Chemistry C*, 2011, **115**, 15282-15287.
28. G. A. Simms, J. D. Padmos and P. Zhang, *The Journal of Chemical Physics*, 2009, **131**, 214703.
29. M. A. MacDonald, P. Zhang, H. Qian and R. Jin, *The Journal of Physical Chemistry Letters*, 2010, **1**, 1821-1825.
30. G. Mark and M. B. Nicholas, *Journal of Physics: Materials*, 2020.
31. Z. Duan, J. Timoshenko, P. Kunal, S. D. House, H. Wan, K. Jarvis, C. Bonifacio, J. C. Yang, R. M. Crooks, A. I. Frenkel, S. M. Humphrey and G. Henkelman, *Nanoscale*, 2018, **10**, 22520-22532.
32. I. Bilecka, P. Elser and M. Niederberger, *ACS Nano*, 2009, **3**, 467-477.
33. T. Dainese, S. Antonello, J. A. Gascón, F. Pan, N. V. Perera, M. Ruzzi, A. Venzo, A. Zoleo, K. Rissanen and F. Maran, *ACS Nano*, 2014, **8**, 3904-3912.
34. A. Shivhare, K. E. Lee, Y. Hu and R. W. J. Scott, *The Journal of Physical Chemistry C*, 2015, **119**, 23279-23284.
35. S. Yamazoe, S. Takano, W. Kurashige, T. Yokoyama, K. Nitta, Y. Negishi and T. Tsukuda, *Nature Communications*, 2016, **7**, 10414.
36. D. J. Morris, R. Yang, T. Higaki, M. J. Ward, R. Jin and P. Zhang, *The Journal of Physical Chemistry C*, 2018, **122**, 23414-23419.
37. V. Petkov, *Materials today*, 2008, **11**, 28-38.
38. S. J. L. Billinge, *Philosophical Transactions of the Royal Society A: Mathematical, Physical and Engineering Sciences*, 2019, **377**, 20180413.
39. N. M. Bedford, Z. E. Hughes, Z. Tang, Y. Li, B. D. Briggs, Y. Ren, M. T. Swihart, V. G. Petkov, R. R. Naik, M. R. Knecht and T. R. Walsh, *Journal of the American Chemical Society*, 2016, **138**, 540-548.
40. D. R. Corey and C. S. Craik, *Journal of the American Chemical Society*, 1992, **114**, 1784-1790.

41. P. Zhao, X. Feng, D. Huang, G. Yang and D. Astruc, *Coordination Chemistry Reviews*, 2015, **287**, 114-136.
42. S. Gu, S. Wunder, Y. Lu, M. Ballauff, R. Fenger, K. Rademann, B. Jaquet and A. Zaccone, *The Journal of Physical Chemistry C*, 2014, **118**, 18618-18625.
43. Y. Li, Z. Tang, P. N. Prasad, M. R. Knecht and M. T. Swihart, *Nanoscale*, 2014, **6**, 3165-3172.
44. H. Yamamoto, H. Yano, H. Kouchi, Y. Obora, R. Arakawa and H. Kawasaki, *Nanoscale*, 2012, **4**, 4148-4154.
45. N. J. Greenfield, *Nat Protoc*, 2006, **1**, 2876-2890.
46. B. Ravel and M. Newville, *Journal of Synchrotron Radiation*, 2005, **12**, 537-541.
47. V. Petkov, *J Appl Crystallogr*, 1989, **22**, 387-389.